Séminaire Laurent Schwartz

EDP et applications

Année 2015-2016

Kazuo Aoki, Ryo Kagaya, Shingo Kosuge, and Hiroaki Yoshida

Numerical analysis of the Taylor-vortex flow of a slightly rarefied gas

Numerical Analysis of the Taylor-Vortex Flow of a Slightly Rarefied Gas

Kazuo Aoki[1], Ryo Kagaya[2], Shingo Kosuge[3], and Hiroaki Yoshida[4]

[1]National Center for Theoretical Sciences, National Taiwan University, Taipei 10617, Taiwan and Department of Mathematics, National Cheng Kung University, Tainan 70101, Taiwan
[2]Department of Mechanical Engineering and Science, Graduate School of Engineering, Kyoto University, Kyoto 615-8540, Japan
[3]Center for Global Leadership Engineering Education, Graduate School of Engineering, Kyoto University, Kyoto 615-8540, Japan
[4]Toyota Central R&D Labs., Inc., Aichi 480-1192, Japan

Abstract The axisymmetric Taylor-vortex flow of a rarefied gas between two coaxial circular cylinders, a rotating inner cylinder and a resting outer one, is investigated numerically for small Knudsen numbers on the basis of the compressible Navier-Stokes (CNS) equations and their appropriate slip boundary conditions. The accuracy of the result as an approximate solution to the Boltzmann equation is confirmed by comparing it with the result obtained by the direct simulation Monte Carlo (DSMC) method for Knudsen numbers of the order of 10^{-2}. The flow field for smaller Knudsen numbers (of the order of 10^{-3}) exhibits a boundary-layer like structure near the cylinders. It is shown that, compared with the cylindrical Couette flow, the velocity slip in the circumferential direction is enhanced in the Taylor-vortex flow.

1   Introduction

The Taylor-vortex flow between two coaxial circular cylinders rotating at different angular velocities is one of the most fundamental problems in fluid dynamics. In particular, for an incompressible fluid, it is a classical problem that has been investigated extensively [1, 2, 3]. As for a rarefied gas, its study is relatively recent, and some results based on the direct simulation Monte Carlo (DSMC) method [4, 5] have been reported in the case of high-speed rotation of the inner cylinder for Knudsen numbers of the order of 10^{-2} and 10^{-3} (e.g., [6, 7, 8, 9]). However, because of the increase of the computational load, there are few studies of detailed flow structure for Knudsen numbers of the order of 10^{-3} and smaller. Therefore, the behavior of the flow field when the Knudsen number approaches zero has not been fully understood.

In the present study, we revisit this problem with special interest in the structure of the flow field and the magnitude of the velocity slip in the near continuum regime. We also use the DSMC method as a numerical tool. However, when the Knudsen number becomes small, it becomes increasingly difficult to obtain detailed structure of the flow field with this method. On the other hand, for small Knudsen numbers,

a systematic asymptotic analysis has been carried out for the Boltzmann equation, and the fluid-dynamic equations and their boundary conditions of slip type that give the correct asymptotic solution for the steady boundary-value problem of the Boltzmann equation have been established in different physical situations (Sone's asymptotic theory, cf. [10, 11, 12, 13]). Such fluid-dynamic systems are much more convenient for numerical analysis of flows at smaller Knudsen numbers. However, the Taylor-Couette flow with high-speed rotation of the inner cylinder does not seem to be covered by these situations where the fluid-dynamic systems are available. Therefore, we are going to use the Navier–Stokes equations for a compressible fluid and their correct slip boundary conditions to investigate the present problem. Their validity is confirmed numerically by the comparison with the result by the DSMC method for Knudsen numbers of the order of 10^{-2}.

It should be mentioned that the Taylor-vortex flow with high-speed rotation of the inner cylinder has been analyzed numerically using the compressible Navier–Stokes equations and the no-slip boundary conditions [14]. The reader is referred to [15, 16] for linear-stability analysis of the high-speed cylindrical Couette flow of a rarefied gas.

2 Problem and assumptions

Let us consider a rarefied gas in an annular domain of height L bounded by two coaxial circular cylinders and top and bottom boundaries. The inner cylinder (radius R_1, temperature T_0) is rotating with a surface speed V_1, whereas the outer cylinder (radius R_2, temperature T_0) is at rest. We investigate the steady behavior of the gas under the following assumptions: (i) The behavior of the gas is described by the Boltzmann equation for hard-sphere molecules; (ii) The gas molecules undergo diffuse reflection on the cylinders and specular reflection on the top and bottom boundaries; (iii) The flow field is axisymmetric; (iv) The Knudsen number (Kn) is small. The DSMC method is used down to Kn = 0.01. But, for smaller Kn (down to Kn = 0.0007), we use the Navier–Stokes equations for a compressible fluid and the correct slip boundary conditions (of the order of Kn) on the cylinders derived consistently with the Chapman–Enskog solution of the Boltzmann equation.

3 Basic equations

Let ρ_0 be the average density of the gas in the annular domain, and let $p_0 = R\rho_0 T_0$, where R is the gas constant per unit mass (i.e., $R = k/m$ with k the Boltzmann constant and m the mass of a molecule). Let us define the Knudsen number Kn as Kn $= l_0/R_1$, where l_0 is the mean free path of the gas molecules in the equilibrium at rest with temperature T_0 and density ρ_0. Then, we introduce dimensionless variables t, $\boldsymbol{x}$, $\boldsymbol{\zeta}$, etc. by means of the following definitions of the corresponding dimensional quantities: $R_1(2RT_0)^{-1/2}t$ is the time variable, $R_1\boldsymbol{x}$ the spatial position vector, $(2RT_0)^{1/2}\boldsymbol{\zeta}$ the molecular velocity, $\rho_0(2RT_0)^{-3/2}f$ the molecular velocity distribution

function, $\rho_0\rho$ the density, $(2RT_0)^{1/2}\boldsymbol{v}$ the flow velocity, T_0T the temperature, p_0p the pressure, and p_0e the total energy per unit volume. In addition, we use the cylindrical coordinate system (r, θ, z) in the dimensionless $\boldsymbol{x}$ space with z axis on the axis of the inner (or outer) cylinder and $z = 0$ on the bottom boundary of the annular domain. Therefore, the gas domain is expressed as $1 \leq r \leq R_2/R_1$, $0 \leq z \leq L/R_1$, and $0 \leq \theta < 2\pi$. We denote the r, θ, and z components of $\boldsymbol{\zeta}$ by ζ_r, ζ_θ, and ζ_z and those of $\boldsymbol{v}$ by v_r, v_θ, and v_z. Our choice of ρ_0 leads to the following normalization condition for the dimensionless density ρ:

$$\frac{2}{(L/R_1)[(R_2/R_1)^2 - 1]} \int_0^{L/R_1} \int_1^{R_2/R_1} \rho r \, dr \, dz = 1, \tag{1}$$

3.1 Boltzmann System

The dimensionless Boltzmann equation in the present axisymmetric problem is expressed as

$$\frac{\partial f}{\partial t} + \zeta_r \frac{\partial f}{\partial r} + \zeta_z \frac{\partial f}{\partial z} + \frac{\zeta_\theta^2}{r} \frac{\partial f}{\partial \zeta_r} - \frac{\zeta_r \zeta_\theta}{r} \frac{\partial f}{\partial \zeta_\theta} = \frac{1}{\varepsilon} J(f, f), \tag{2}$$

where $J(f, f)$ is the collision integral determined by the model of the molecular interaction, the explicit form of which is omitted here for brevity, and $\varepsilon = (\sqrt{\pi}/2)\mathrm{Kn}$.

The dimensionless form of the diffuse-reflection condition on the inner and outer cylinders can be written as

$$f = \pi^{-3/2}\sigma_w \exp\left(-[\zeta_r^2 + (\zeta_\theta - V_w)^2 + \zeta_z^2]\right) \qquad \text{for} \quad \zeta_n > 0, \tag{3a}$$

$$\sigma_w = -2\pi^{1/2} \int_{\zeta_n < 0} \zeta_n f \, d\boldsymbol{\zeta}, \tag{3b}$$

where we let $V_w = V_1/(2RT_0)^{1/2}$ and $\zeta_n = \zeta_r$ on the inner cylinder ($r = 1$, $0 \leq z \leq L/R_1$) and $V_w = 0$ and $\zeta_n = -\zeta_r$ on the outer ($r = R_2/R_1$, $0 \leq z \leq L/R_1$). On the other hand, the specular reflection condition on the top ($z = L/R_1$) and bottom ($z = 0$) boundaries is given by

$$f(t, r, z, \zeta_r, \zeta_\theta, \zeta_z) = f(t, r, z, \zeta_r, \zeta_\theta, -\zeta_z), \tag{4}$$

for $\zeta_z > 0$ on $z = 0$ and for $\zeta_z < 0$ on $z = L/R_1$.

The initial condition is given by

$$f = f_0 \qquad \text{at} \quad t = 0, \tag{5}$$

where f_0 is an appropriately chosen initial function (e.g., the Maxwellian distribution corresponding to the gas at rest with temperature T_0 and density ρ_0).

3.2 Navier–Stokes System

If we take the Chapman–Enskog solution of the Boltzmann equation (2) and retain the terms of $O(\mathrm{Kn})$ neglecting the higher-order terms, we have the Navier–Stokes

equation for a compressible fluid (cf. Sec. B.4 in [13]), which may be written in the following form:

$$\frac{\partial \rho}{\partial t} + \nabla \cdot (\rho \boldsymbol{v}) = 0, \tag{6a}$$

$$\frac{\partial}{\partial t}(\rho \boldsymbol{v}) + \nabla \cdot (\rho \boldsymbol{v}\boldsymbol{v}) + \frac{1}{2}\nabla p = \frac{1}{2}\nabla \cdot \underline{\tau}, \tag{6b}$$

$$\frac{\partial e}{\partial t} + \nabla \cdot [(e + p)\boldsymbol{v}] = \nabla \cdot (\underline{\tau} \cdot \boldsymbol{v}) - \nabla \cdot \boldsymbol{q}. \tag{6c}$$

where $p_0 \underline{\tau}$ and $p_0(2RT_0)^{1/2}\boldsymbol{q}$ are, respectively, the dimensional viscous-stress tensor and heat-flow vector, and e, $\underline{\tau}$, and $\boldsymbol{q}$ are given as follows:

$$e = \rho[(3/2)\,T + |\boldsymbol{v}|^2], \tag{7a}$$

$$\underline{\tau} = \varepsilon\gamma_1 T^{1/2}[\nabla\boldsymbol{v} + (\nabla\boldsymbol{v})^{\mathrm{T}} - (2/3)(\nabla \cdot \boldsymbol{v})\,\underline{I}], \tag{7b}$$

$$\boldsymbol{q} = -(5/4)\varepsilon\gamma_2 T^{1/2}\nabla T, \tag{7c}$$

where $(\ \ )^{\mathrm{T}}$ indicates the transpose operation, $\underline{I}$ denotes the unit tensor, and γ_1 and γ_2 are functions of T depending on the model of molecular interaction and are constant for hard-sphere molecules ($\gamma_1 = 1.270042$ and $\gamma_2 = 1.922284$ [12, 13]). The terms $\varepsilon\gamma_1 T^{1/2}$ and $\varepsilon\gamma_2 T^{1/2}$ in Eqs. (7b) and (7c) correspond, respectively, to the viscosity and thermal conductivity of the gas. Equations (6) and (7) form a closed set of equations together with the equation of state, $p = \rho T$. In Eqs. (6) and (7), the cylindrical coordinates are not used, so that the axial symmetry is not shown explicitly.

On the basis of the first-order Chapman–Enskog solution, we can derive the slip boundary conditions on the cylinders appropriate to the Navier–Stokes equations (6) (see the next subsection), which are written in the following form: At $r = R_w$,

$$v_r = 0, \qquad \rho(v_\theta - V_w) = -\delta k_0 \left(\frac{\partial v_\theta}{\partial r} - \frac{V_w}{R_w}\right)\varepsilon, \qquad \rho v_z = -\delta k_0 \frac{\partial v_z}{\partial r}\varepsilon, \tag{8a}$$

$$\rho(T - 1) = \delta d_1 \frac{\partial T}{\partial r}\varepsilon. \tag{8b}$$

Here, we let $R_w = 1$, $V_w = V_1/(2RT_0)^{1/2}$, and $\delta = 1$ for the inner cylinder ($r = 1$, $0 \le z \le L/R_1$) and $R_w = R_2/R_1$, $V_w = 0$, and $\delta = -1$ for the outer ($r = R_2/R_1$, $0 \le z \le L/R_1$); k_0 and d_1 are the so-called slip coefficients and known to be $k_0 = -1.2540$ and $d_1 = 2.4001$ for hard-sphere molecules and the diffuse reflection condition [12, 13].

We also impose appropriate conditions corresponding to the specular reflection (4) on the top and bottom boundaries, that is,

$$\frac{\partial v_r}{\partial z} = \frac{\partial v_\theta}{\partial z} = v_z = 0, \qquad \frac{\partial T}{\partial z} = 0, \qquad \text{at}\quad z = 0 \quad \text{and}\quad L/R_1. \tag{9}$$

The initial condition that we use in the present study is the uniform state at rest ($\rho = T = 1$, $\boldsymbol{v} = 0$) or the steady solution for a nearby ε.

3.3 Derivation of Slip Boundary Conditions

If we denote the Chapman–Enskog solution of the Boltzmann equation (2) by $f_{\mathrm{CE}} = f_{\mathrm{CE}}^{(0)} + f_{\mathrm{CE}}^{(1)}\varepsilon + O(\varepsilon^2)$, we are using the part $f_{\mathrm{CE}}^{(0)} + f_{\mathrm{CE}}^{(1)}\varepsilon$. The leading-order term $f_{\mathrm{CE}}^{(0)}$, which is the local Maxwellian distribution with density ρ, flow velocity $\boldsymbol{v}$, and temperature T, satisfies the boundary condition (3) if we assume that $v_r = v_z = 0$, $v_\theta = V_w$, and $T = 1$ on the cylinders. On the other hand, the functional form of $f_{\mathrm{CE}}^{(1)}$ with respect to $\boldsymbol{\zeta}$ is different from that of the boundary condition (3), so that $f_{\mathrm{CE}}^{(1)}$ has no freedom to satisfy the boundary condition. Therefore, we seek the solution satisfying the boundary condition in the form $f = f_{\mathrm{CE}} + f_{\mathrm{K}}$, where f_{K} is the correction term appreciable only in the Knudsen layers, i.e., the thin layers with thickness of $O(\varepsilon)$, adjacent to the inner and outer cylinders [12, 13]. More specifically, f_{K} has the length scale of variation of $O(\varepsilon)$ in the direction normal to the surface of the cylinders, so that f_{K} is expressed as $f_{\mathrm{K}}(t, \eta, z, \zeta_n, \zeta_\theta, \zeta_z)$, where $\eta = (r-1)/\varepsilon$, $\zeta_n = \zeta_r$ in the Knudsen layer at the inner cylinder and $\eta = (R_2/R_1 - r)/\varepsilon$, $\zeta_n = -\zeta_r$ in that at the outer, and is assumed to vanish rapidly as $\eta \to \infty$.

Because $f_{\mathrm{CE}}^{(0)}$ can satisfy the boundary condition (3) with the choice $v_r = v_z = 0$, $v_\theta = V_w$, and $T = 1$ on the cylinders, we may consider that $v_r = v_z = O(\varepsilon)$, $v_\theta - V_w = O(\varepsilon)$, and $T - 1 = O(\varepsilon)$. Therefore, we assume the form $f_{\mathrm{K}} = f_{\mathrm{K}}^{(1)}\varepsilon + O(\varepsilon^2)$ and try to obtain $f_{\mathrm{K}}^{(1)}$. We now substitute $f = f_{\mathrm{CE}} + f_{\mathrm{K}}$ into the Boltzmann equation (2) in the Knudsen layers and the boundary condition (3). If we take into account the properties of f_{CE} and f_{K} and neglect the quantities of $O(\varepsilon^2)$ and higher, we obtain the equation and boundary condition for $f_{\mathrm{K}}^{(1)}$. They are essentially the same as the Knudsen-layer problem encountered in the linear asymptotic theory (cf. Sec 3.1 in [13]) and are decomposed into two classical half-space problems, the shear-slip and the temperature-jump problems. By solving these problems, the slip boundary conditions (8), including the values of the slip coefficients, are obtained together with the solution $f_{\mathrm{K}}^{(1)}$. Numerical solutions of these problems are available in the literature (e.g., [17, 18]).

4 Numerical analysis and results

We solve the Boltzmann system (2)–(5) numerically by the DSMC method [4, 5]. As for the Navier–Stokes system, Eqs. (6)–(9) and the initial condition, we use the Beam–Warming method [19] for the time evolution and the forth-order central differences for the finite difference in space. When we use the uniform state at rest ($\rho = T = 1$, $\boldsymbol{v} = 0$) as the initial condition, it is slightly perturbed by adding $v_z = \sin(\pi z/L)/1000$. For both systems, the steady solution is obtained as the long-time limit by pursuing the time evolution of the solution.

In the present paper, we fix the parameters R_2/R_1, L/R_1, and $V_1/(2RT_0)^{1/2}$ as $R_2/R_1 = 2$, $L/R_1 = 1$, and $V_1/(2RT_0)^{1/2} = 1$ and show the results for different $\mathrm{Kn}\,[=(2/\sqrt{\pi})\,\varepsilon]$.
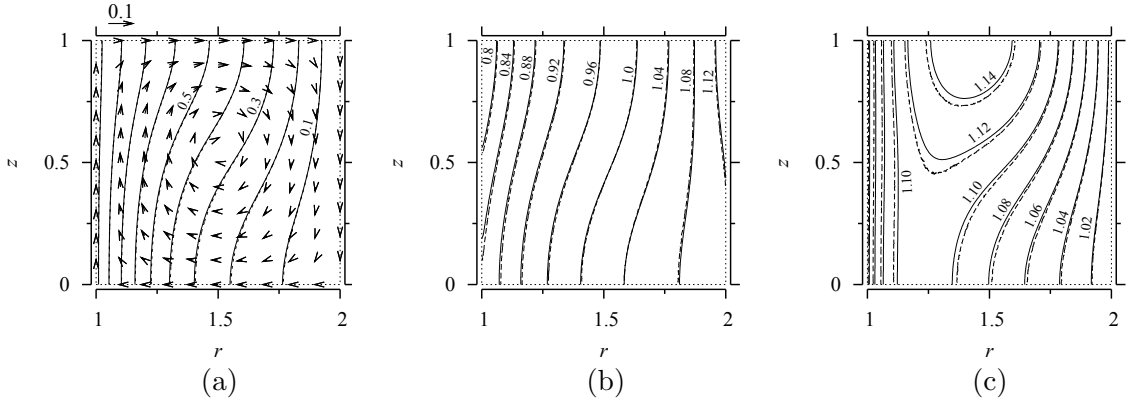
Fig. 1: Comparison between the compressible Navier–Stokes (CNS) result and the DSMC result for Kn = 0.02. (a) Contour lines of v_θ and the vector (v_r, v_z) in the rz plane, (b) contour lines of ρ, (c) contour lines of T. The solid (dashed) line indicates the CNS (DSMC) result. The arrow indicates (v_r, v_z) at its starting point (CNS result), and its scale is shown above the figure.
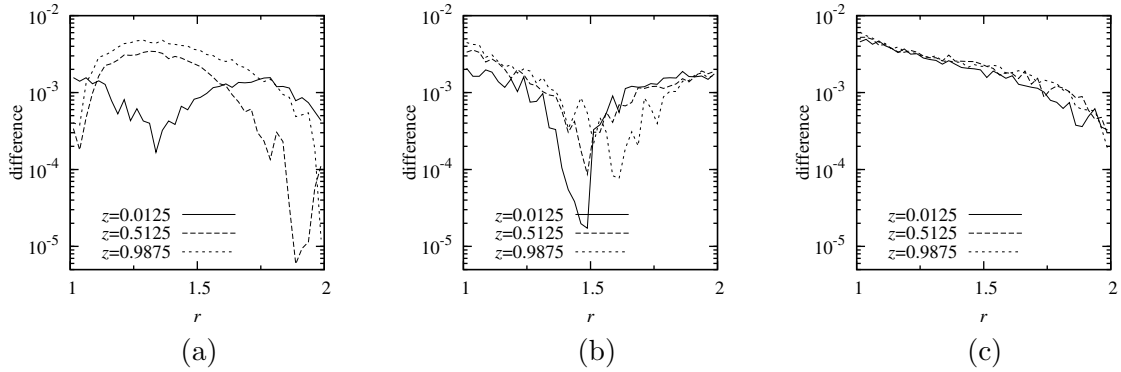

Fig. 2: Difference between the CNS and DSMC results in macroscopic quantities at $z = 0.0125, 0.5125, 0.9875$ for Kn = 0.02. (a) $|v_\theta^{\mathrm{CNS}} - v_\theta^{\mathrm{DSMC}}|$, (b) $|\rho^{\mathrm{CNS}} - \rho^{\mathrm{DSMC}}|$, (c) $|T^{\mathrm{CNS}} - T^{\mathrm{DSMC}}|$.

4.1 Comparison between the Boltzmann and Navier–Stokes Systems

We first compare the flow field obtained for the compressible Navier–Stokes system (CNS) and that for the Boltzmann system by the DSMC method.

Figure 1 shows the results for Kn = 0.02: Fig. 1(a) shows the contour lines of v_θ and the two-dimensional vector (v_r, v_z) in the rz plane, Fig. 1(b) the contour lines of ρ, and Fig. 1(c) the contour lines of T. The solid line indicates the contour line obtained for CNS and the dashed line that by the DSMC method; the arrow in Fig. 1 indicates (v_r, v_z) for CNS at its starting point, and its scale is shown above the figure. Figure 2 is a plot of the distribution in r of the difference (absolute value) in the macroscopic quantities along the three lines $z = 0.0125, 0.5125,$ and 0.9875: Fig. 2(a) shows $|v_\theta^{\mathrm{CNS}} - v_\theta^{\mathrm{DSMC}}|$, Fig. 2(b) $|\rho^{\mathrm{CNS}} - \rho^{\mathrm{DSMC}}|$, and Fig. 2(c)
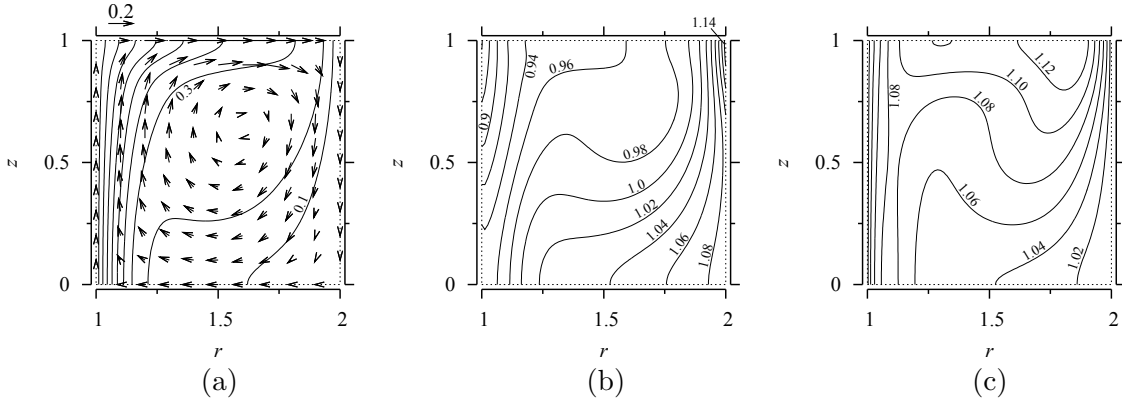
Fig. 3: Flow field at Kn = 0.005 (CNS). (a) Contour lines of v_θ and the vector (v_r, v_z) in the rz plane, (b) contour lines of ρ, (c) contour lines of T. The arrow indicates (v_r, v_z) at its starting point, and its scale is shown above the figure.

$|T^{\mathrm{CNS}} - T^{\mathrm{DSMC}}|$, where the superscript CNS indicates the CNS results, and the superscript DSMC the DSMC result. Since the DSMC result contains statistical fluctuation, the curves in Fig. 2 are not smooth.

In Fig. 1, one observes the Taylor-vortex flow with a single roll. The distributions of the circumferential velocity and density obtained by both methods agree well [Figs. 1(a) and 1(b)], but a slight discrepancy is seen for the isothermal lines [Fig. 1(c)]. This is due to the fact that the difference is magnified because of the small temperature variation. As seen in Fig. 2, the discrepancy is of $O(10^{-3})$. Since the CNS result is based on the first-order Chapman–Enskog solution, its expected deviation from the DSMC result may be of $O(\mathrm{Kn}^2)$, that is, $O(4 \times 10^{-4})$ [since the Knudsen layer corrections are not made for the CNS result, the discrepancy inside the Knudsen layers can be of $O(\mathrm{Kn})$]. The discrepancy shown by Fig. 2 is larger by one order of magnitude. The reason will be mentioned in DISCUSSIONS. Naturally, we have better agreement between CNS and DSMC results for Kn = 0.01, the results for which are not shown in the present paper.

4.2   Flow Field Obtained by the Navier–Stokes System

In Figs. 3 and 4, we show the results for Kn = 0.005 and 0.001, respectively: As in Fig. 1, Figs. 3(a) and 4(a) show the contour lines of v_θ and the velocity vector (v_r, v_z) on the rz plane, Figs. 3(b) and 4(b) the contour lines of ρ, and Figs. 3(c) and 4(c) the contour lines of T. The Taylor-vortex flow with a single vortex is induced in both cases. The concentration of the contour lines near the cylinders indicates that the gradients of v_θ, ρ, and T are steep there (in particular, near the inner cylinder) and are mild in the bulk of the gas. The gradients near the cylinders are steeper at Kn = 0.001. Since the viscosity is smaller for smaller Kn, this feature suggests that the structure like the viscous boundary layer appears in the vicinity of the cylinders.

In order to look into the boundary-layer like structure, we show in Figs. 5–7 the profile of v_θ for Kn = 0.01, 0.005, and 0.001 along the three lines, $z = 0$ (Fig. 5),
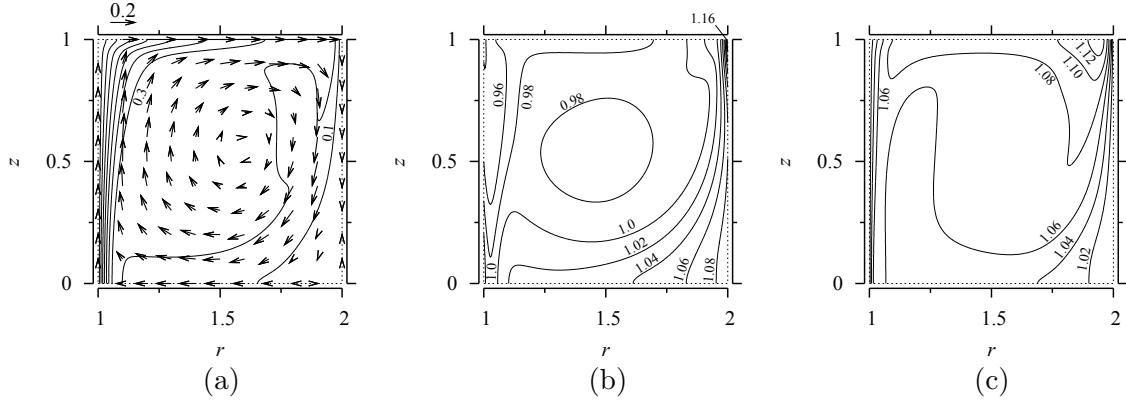
Fig. 4: Flow field at $\mathrm{Kn} = 0.001$ (CNS). (a) Contour lines of v_θ and the vector (v_r, v_z) in the rz plane, (b) contour lines of ρ, (c) contour lines of T. The arrow indicates (v_r, v_z) at its starting point, and its scale is shown above the figure.
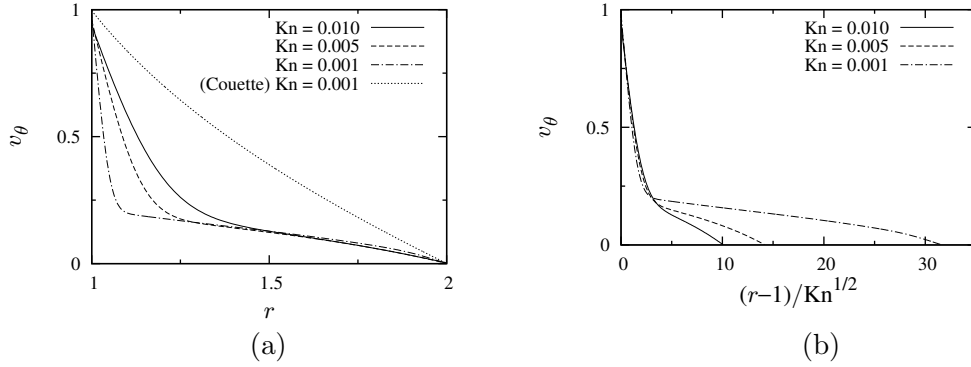

Fig. 5: Profile of v_θ along $z = 0$ (CNS). (a) v_θ vs r, (b) v_θ vs the stretched radial coordinate $(r - 1)/\mathrm{Kn}^{1/2}$ measured from the inner cylinder. In (a), v_θ for the cylindrical Couette flow at $\mathrm{Kn} = 0.001$ is also shown.

Fig. 6: Profile of v_θ along $z = 0.5$ (CNS). (a) v_θ vs r, (b) v_θ vs the stretched radial coordinate $(r - 1)/\mathrm{Kn}^{1/2}$ measured from the inner cylinder. In (a), v_θ for the cylindrical Couette flow at $\mathrm{Kn} = 0.001$ is also shown.
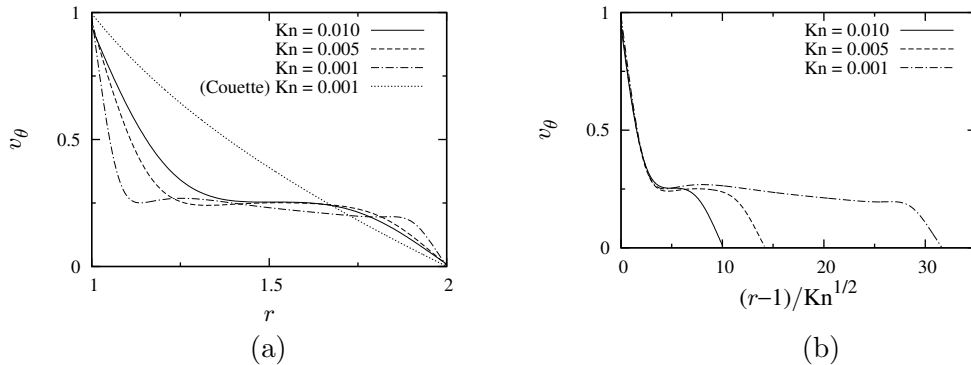
Fig. 7: Profile of v_θ along $z = 1$ (CNS). (a) v_θ vs r, (b) v_θ vs the stretched radial coordinate $(r - 1)/\mathrm{Kn}^{1/2}$ measured from the inner cylinder. In (a), v_θ for the cylindrical Couette flow at $\mathrm{Kn} = 0.001$ is also shown.
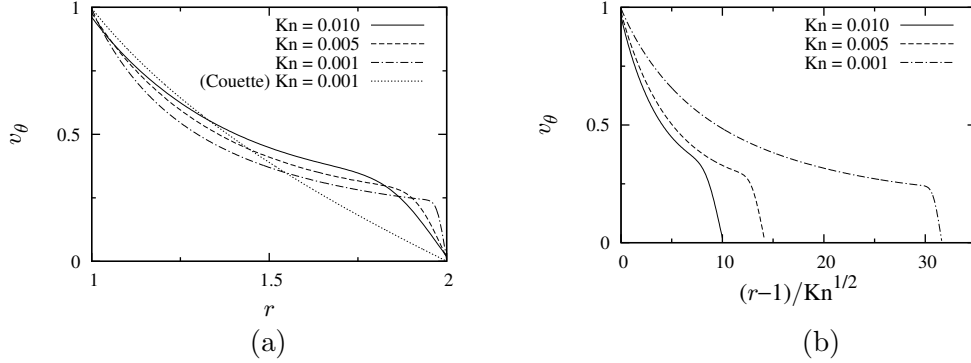
$z = 0.5$ (Fig. 6), and $z = 1$ (Fig. 7). Let us focus our attention on the profile near the inner cylinder. In each figure, panel (a) is the ordinary profile, and panel (b) the profile as a function of the stretched radial coordinate $(r - 1)/\mathrm{Kn}^{1/2}$ measured from the inner cylinder ($r = 1$). In panel (a), the profile of v_θ for the cylindrical Couette flow at $\mathrm{Kn} = 0.001$ is also shown. The profiles at $z = 0$ [Fig. 5(a)] and 0.5 [Fig. 6(a)] show that, as Kn becomes small, the gradient of v_θ becomes steeper near the inner cylinder but becomes milder in the bulk of the gas. As the result, the profiles differ significantly from that of the cylindrical Couette flow. Moreover, as seen from Figs. 5(b) and 6(b), the profiles near the inner cylinder at three different Knudsen numbers exhibit a similarity in the sense that they more or less coincide in the stretched radial coordinate $(r - 1)/\mathrm{Kn}^{1/2}$. This suggests that the viscous boundary-layer structure appears, since $\mathrm{Kn} \propto 1/\mathrm{Re}$ with Re the Reynolds number. The latter relation is the consequence of the von Kármán relation $\mathrm{Ma} \propto \mathrm{Kn}\,\mathrm{Re}$ with Ma the Mach number and of the fact that $\mathrm{Ma} \propto V_1/(2RT_0)^{1/2} = 1$ in Figs. 5–7. In contrast, the profile at $z = 1$ does not differ much from the cylindrical Couette flow, and the similarity seen at $z = 0$ and 0.5 is not observed. This is because the outward radial flow ($v_r > 0$) near $z = 1$ [cf. Figs. 3(a) and 4(a)] lifts up the boundary layer and destroys the boundary-layer structure.

If we look at Figs. 5(a) and 6(a) carefully, we notice that the velocity slip $V_1/(2RT_0)^{1/2} - v_\theta = 1 - v_\theta$ on the inner cylinder ($r = 1$) becomes much larger, compared to the cylindrical Couette flow, once the Taylor vortex is formed. Figure 8(a) shows the velocity slip $1 - v_\theta$ on the inner cylinder at $z = 0$ [cf. Fig. 5(a)] versus Kn. The solid line indicates the result for the cylindrical Couette flow obtained under the constraint of axial and circumferential uniformity, and ∘ indicates the results for axisymmetric computation. As Kn is reduced from 0.04, the velocity slip bifurcates at $\mathrm{Kn} \approx 0.023$ at which the Taylor vortex is formed. Figure 8(b) is a closeup of Fig. 8(a) near the bifurcation point. Figure 8(c) is the replot of Fig. 8(a) in log-log scale. The velocity slip in the cylindrical Couette flow tends to follow the line with gradient 1, which means that $1 - v_\theta \propto \mathrm{Kn}$, whereas that for
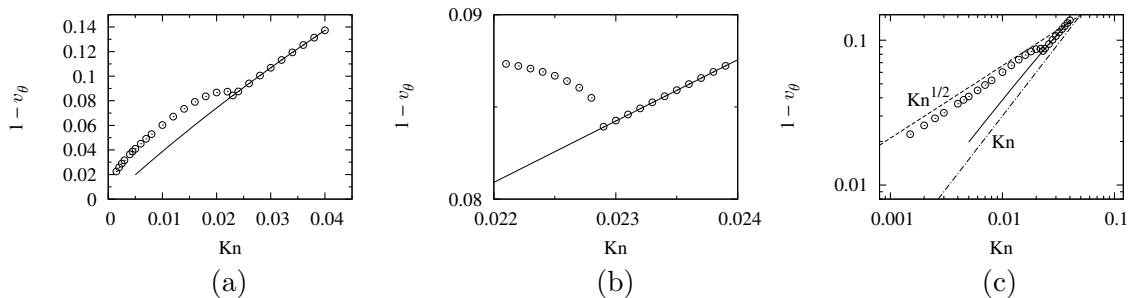
Fig. 8: Velocity slip $V_1/(2RT_0)^{1/2} - v_\theta = 1 - v_\theta$ at $z = 0$ on the inner cylinder $(r = 1)$ (CNS). (a) $1 - v_\theta$ vs Kn, (b) closeup of panel (a) near the bifurcation point, (c) $1 - v_\theta$ vs Kn in log-log scale.

the Taylor-vortex flow tends to follow the line with gradient $1/2$, which means that $1 - v_\theta \propto \mathrm{Kn}^{1/2}$. This behavior might seem to contradict the use of the first-order slip boundary conditions (8). This point will be discussed in the following section.

5   Discussions

Let us focus our attention on the structure of the flow field near the inner cylinder. Let us suppose that a boundary-layer like structure, the length scale of which in r direction is $\mathrm{Kn}^{1/2}$, is formed on a part of the inner cylinder. Then, if we use the stretched normal coordinate $y = (r - 1)/\mathrm{Kn}^{1/2}$, the term containing $\partial v_\theta/\partial r$ in Eq. (8a) becomes

$$-k_0 \frac{\partial v_\theta}{\partial r} \varepsilon = -\frac{\sqrt{\pi}}{2} k_0 \frac{\partial v_\theta}{\partial y} \mathrm{Kn}^{1/2}. \tag{10}$$

That is, this term is upgraded to $O(\mathrm{Kn}^{1/2})$ by the presence of the boundary layer. The same is true for the other two terms, $-k_0(\partial v_z/\partial r)\,\varepsilon$ and $d_1(\partial T/\partial r)\,\varepsilon$, in Eq. (8). This is consistent with the magnitude of the velocity slip shown in Fig. 8(c) and thus provides another piece of evidence of the boundary-layer structure at least near $z = 0$.

Since we are using the first-order Chapman–Enskog solution corresponding to the Navier–Stokes equations, we expect that our numerical solution using the latter equation is a correct approximation to the solution of the Boltzmann equation up to $O(\mathrm{Kn})$. In other words, we have neglected the terms of $O(\mathrm{Kn}^2)$, the so-called Burnett terms, in the fluid-dynamic equations, which may contain higher-order derivatives, such as $(1/r)(\partial^3 T/\partial r^2 \partial \theta)\varepsilon^2$. The latter term may be upgraded as $(1/r)(\partial^3 T/\partial y^2 \partial \theta)\mathrm{Kn}$ inside the boundary layer. In consequence, the Navier–Stokes equations do not guarantee the accuracy up to $O(\mathrm{Kn})$ inside the boundary layer. This may be one of the reasons that the deviation of the CNS solution from the DSMC result (Fig. 2) is of $O(\mathrm{Kn}^{3/2})$ and is larger than the expected difference of

$O(\text{Kn}^2)$. However, on the contrary to the above observation, the CNS result seems to be accurate up to $O(\text{Kn})$ (Fig. 2).

Once the viscous boundary layer is formed near the cylinders, the correct asymptotic solution and the corresponding fluid-dynamic equations would be obtained by the scheme for finite Mach numbers of Sone's asymptotic analysis [20] (cf. Chap. 6 in [12]). It is carried out with $\text{Kn}^{1/2}$ as the small parameter. It gives the shear-slip and temperature jump conditions at $O(\text{Kn}^{1/2})$ on the boundary and guarantees that the CNS equations are correct up to $O(\text{Kn}^{1/2})$. It is consistent with our numerical result and intuitive argument. However, this type of systematic asymptotic analysis is not applicable uniformly because, as seen from Figs. 3–7, the boundary-layer structure does not cover the whole inner (outer) cylinder ($0 \leq z \leq 1$). Therefore, it is not obvious how to derive the correct and uniformly valid fluid-dynamic system describing the Taylor-vortex flow from the Boltzmann system by means of a systematic asymptotic analysis for small Knudsen numbers.

References

[1] G. I. Taylor, *Phil. Trans. R. Soc. London Ser. A* **223**, 289 (1923).

[2] S. Chandrasekhar, *Hydrodynamic and Hydromagnetic Stability*, Oxford University Press, London, 1961.

[3] P. Chossat and G. Iooss, *The Couette-Taylor Problem*, Springer-Verlag, New York, 1994.

[4] G. A. Bird, *Molecular Gas Dynamics*, Oxford University Press, Oxford, 1976.

[5] G. A. Bird, *Molecular Gas Dynamics and the Direct Simulation of Gas Flows*, Oxford University Press, Oxford, 1994.

[6] S. Stefanov and C. Cercignani, *J. Fluid Mech.* **256**, 199 (1993).

[7] D. Riechelmann and K. Nanbu, *Phys. Fluids A* **5**, 2585 (1993).

[8] G. A. Bird, in *Rarefied Gas Dynamics*, edited by C. Shen, Peking University Press, Beijing, 1997, p.149.

[9] K. Aoki, Y. Sone, and M. Yoshimoto, in *Rarefied Gas Dynamics*, edited by R. Brun, R. Campargue, R. Gatignol, J.-C. Lengrand, Cépaduès-Éditions, Toulouse, 1999, Vol. 2, p.109.

[10] Y. Sone, in *Rarefied Gas Dynamics*, edited by L. Trilling and H. Y. Wachman, Academic Press, New York, 1969, p. 243.

[11] Y. Sone, in *Rarefied Gas Dynamics*, edited by D. Dini, Editrice Tecnico Scientifica, Pisa, 1971, Vol. 2, p. 737.

[12] Y. Sone, *Kinetic Theory and Fluid Dynamics*, Birkhäuser, Boston, 2002.

[13] Y. Sone, *Molecular Gas Dynamics: Theory, Techniques, and Applications*, Birkhäuser, Boston, 2007.

[14] B. Larignon, K. Marr, and D. B. Goldstein, *J. Therm. heat Trans.* **20**, 544 (2006).

[15] H. Yoshida and K. Aoki, *Phys. Rev. E* **73**, 021201 (2006).

[16] A. Manela and I. Frankel, *J. Fluid. Mech.* **588**, 59 (2007).

[17] T. Ohwada, Y. Sone, and K. Aoki, *Phys. Fluids A* **1**, 1588 (1989).

[18] Y. Sone, T. Ohwada, and K. Aoki, *Phys. Fluids A* **1**, 236 (1989).

[19] R. M. Beam and R. F. Warming, *AIAA J.* **16**, 393 (1978).

[20] Y. Sone, C. Bardos, F. Golse, and H. Sugimoto, *Eur. J. Mech. B/Fluids* **19**, 325 (2000).